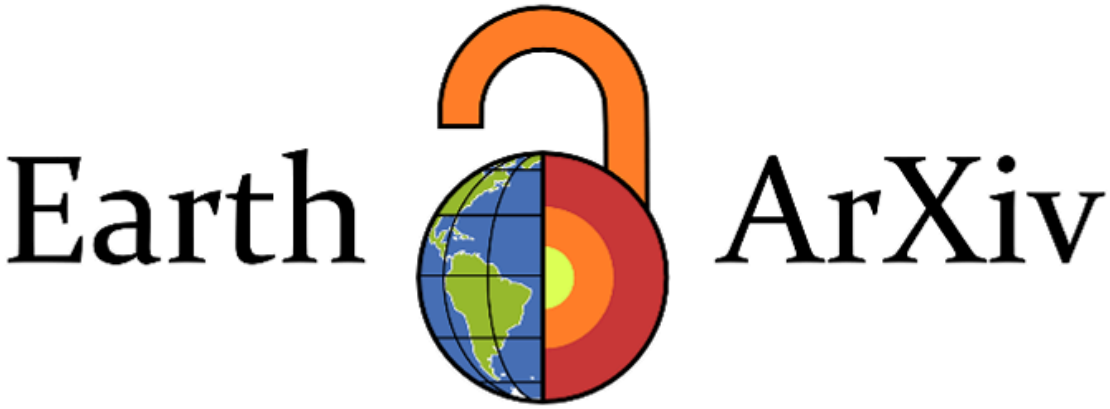



# Mangrove Loss and Growing Coastal Flood Exposure in East Malaysia: A Multi-Decadal Analysis with Sea Level Rise Projections

Author name: Lik Ren, Tai
Affiliation: Woosong University, Daejeon, Korea
Email address: likrentai@gmail.com
ORCID: 0009-0002-6667-3331

# Mangrove Loss and Growing Coastal Flood Exposure in East Malaysia: A Multi-Decadal Analysis with Sea Level Rise Projections

Lik Ren Tai[a]*

[a] *Woosong University, Daejeon, Korea (ORCID iD: 0009-0002-6667-3331)*

---

## Abstract

Mangrove forests provide critical coastal flood protection, yet their ongoing loss in combination with sea level rise creates a compounding exposure dynamic that remains poorly quantified at sub-national scale across Southeast Asia. This study presents the first systematic, multi-decadal analysis of mangrove loss and coastal flood exposure change for the 10 km coastal buffer of East Malaysia (Sabah and Sarawak), covering 1996 to 2020 and projecting forward to 2050 under a structured scenario matrix. Drawing on five openly available global datasets — the Global Mangrove Watch v3.0, Copernicus GLO-30 digital elevation model, WorldPop 2020 population grid, GADM v4.1 administrative boundaries, and IPCC AR6 sea level projections — and a reproducible Python-based workflow, the study quantifies mangrove extent change, hydrologically-connected inundation zones at five elevation thresholds, flood exposure attributable to historical loss, and population exposure under six combined mangrove loss and sea level rise scenarios. Net mangrove loss of 46.34 km² (−1.14%) was recorded over the study period, masking a gross loss of 114.06 km². Four spatial hotspots were identified: the Rajang Delta, SW Sarawak coast, Menumbok Forest Reserve and Kinabatangan coast. Historical mangrove loss exposed an additional 43.79 to 52.14 km² of coastline to inundation, affecting approximately 10,200 to 12,730 people. Scenario projections to 2050 demonstrate that mangrove management trajectory exerts a substantially greater influence on future flood exposure than the choice of emissions scenario, with the spread across mangrove loss scenarios (~29 km², ~12,400 people) exceeding the SSP2-4.5 to SSP5-8.5 spread by more than an order of magnitude. These findings underscore the value of mangrove conservation as a near-term, nature-based coastal adaptation measure in the Indo-Pacific region.

Keywords: Mangrove loss; coastal flood exposure; sea level rise; East Malaysia; nature-based adaptation; inundation modelling; blue carbon

Article highlights:

- Net mangrove loss of 46.34 km² recorded in East Malaysia's coastal buffer, 1996–2020
- Four loss hotspots identified including the Rajang Delta and Menumbok Forest Reserve
- Historical loss exposed 43.79–52.14 km² of additional coastline to inundation risk
- Mangrove management trajectory dominates over SLR scenario choice at 2050 horizon
- Reproducible open-source workflow transferable to other Indo-Pacific mangrove coastlines

---

## 1. Introduction

### 1.1 Background and Motivation

Coastal ecosystems are among the most densely settled and rapidly changing environments on Earth. Approximately one in ten people worldwide, representing between 680 and 900 million individuals, live in the Low Elevation Coastal Zone, broadly defined as land situated less than 10 m above sea level [1]. Against this backdrop, sea level rise driven by climate change poses an escalating threat to coastal communities, infrastructure and ecosystems. Kulp and Strauss [6] estimated that by 2050, land currently occupied by approximately 300 million people will fall below the elevation of average annual coastal flood events, with

Southeast Asia among the most heavily exposed regions owing to the combination of low-lying deltaic and estuarine coastlines, dense coastal settlement and relatively modest adaptive capacity in many areas.

Mangrove forests occupy a critical position at the land-sea interface in tropical and subtropical coastal systems. Beyond their well-documented roles in carbon sequestration, fisheries support and biodiversity conservation [13], mangroves provide a direct and quantifiable biophysical service to coastal communities: the attenuation of wave energy, reduction of storm surge propagation and stabilisation of shorelines against erosion [3, 15]. Menéndez et al. [2] estimated, using spatially explicit hydrodynamic and economic models, that mangroves globally provide flood protection benefits exceeding US$65 billion per year and shield approximately 15 million people from flooding annually. Temmerman et al. [3] demonstrated that tidal wetlands, including mangroves, are particularly effective in attenuating short-period, storm-induced waves, though their capacity to reduce long-period storm surges is more variable and condition-dependent. Together, this body of evidence positions mangrove conservation and restoration as a cost-effective, nature-based approach to coastal adaptation in the face of rising seas.

Yet mangrove forests continue to be lost at significant rates globally, driven principally by conversion to aquaculture, agricultural expansion and coastal development [14, 18]. Richards and Friess [18] estimated an average annual loss rate of 0.18% across Southeast Asia between 2000 and 2012, with oil palm expansion identified as a key but underappreciated driver in Malaysia and Indonesia. Goldberg et al. [16] found that whilst global rates of human-driven mangrove loss declined by 73% between 2000 and 2016, anthropogenic loss hotspots persist across the Indo-Pacific. Worthington et al. [5] demonstrated that advances in remote sensing and big data approaches, including the GMW dataset used in this study, have substantially improved the capacity to monitor mangrove extent and target conservation investment at global scale. Every hectare of mangrove lost from the coastal fringe represents a net reduction in natural buffering capacity, a reduction that becomes progressively more consequential as sea levels rise.

The intersection of ongoing mangrove loss and escalating sea level rise creates a compounding dynamic that remains poorly quantified at the sub-national, coastline-specific scale in many parts of Southeast Asia. Most existing assessments of coastal flood exposure treat the landscape as static, overlooking the role of ecosystem change in modifying exposure over time. Quantifying this dynamic, from retrospective historical analysis through to forward-looking projections, is essential for evidence-based coastal risk management and conservation policy.

East Malaysia, comprising the states of Sabah and Sarawak on the island of Borneo, represents a particularly important case study for this line of inquiry. Together, these two states hold approximately 82% of Malaysia's national mangrove extent [4], with mangroves concentrated along the estuarine and deltaic coastlines of Sarawak and the east-facing Sabah coast. Despite formal protection of the majority of this mangrove estate within Permanent Forest Reserves and designated conservation areas, ongoing loss has been documented in association with oil palm expansion, aquaculture development and coastal land conversion [18]. Simultaneously, the low-lying coastal plains of Sabah and Sarawak, including the extensive deltas of the Rajang, Baram and Kinabatangan rivers, are vulnerable to even modest increases in sea level. The region's coastal communities, including both indigenous groups with deep ties to mangrove-fringing waterways and urban populations in the growing coastal cities of Kuching, Miri, Kota Kinabalu and Sandakan, face a growing but poorly quantified coastal flood risk.

Despite its significance, East Malaysia has not previously been the subject of a systematic, multi-decadal analysis linking observed mangrove loss to quantified changes in coastal flood exposure. The broader Malaysian literature on mangrove change has focused primarily on extent mapping and driver identification rather than on the downstream consequences for coastal flood risk [12, 18]. Coastal flood exposure studies in Southeast Asia have generally operated at coarser spatial scales, using global datasets that do not resolve the sub-regional dynamics of mangrove loss and inundation along specific coastlines [6]. This study addresses that gap directly.

### 1.2 Research Objectives

This study aims to quantify the extent to which mangrove loss along the coastlines of Sabah and Sarawak has increased coastal flood exposure between 1996 and 2020, and to project how continued loss may amplify this exposure under IPCC AR6 sea level rise scenarios to 2050. The analysis is conducted entirely using freely available global datasets and open-source Python-based tools, with the goal of producing a reproducible and transferable methodology applicable to other mangrove-holding coastlines in the region. Three specific research questions are addressed:

1. Where and at what rate have mangroves been lost along the East Malaysian coastline between 1996 and 2020, and what is the spatial distribution of loss hotspots?
2. How has the removal of mangrove cover changed the area and population directly exposed to defined sea level rise inundation thresholds within the 10 km coastal buffer?
3. Under plausible continuation of observed mangrove loss trends, how would coastal flood exposure and population exposure evolve by 2050 under low, intermediate and high emissions sea level rise scenarios?

The study makes three principal contributions to the literature. First, it provides the first systematic, coastline-specific quantification of loss-driven flood exposure change for East Malaysia, linking observed mangrove dynamics to modelled inundation zones at multiple sea level thresholds. Second, it introduces and applies an empirically derived loss-to-exposure ratio that translates projected mangrove loss directly into projected flood exposure, offering a tractable metric for near-term coastal risk assessment. Third, it demonstrates that within the 2050 planning horizon, mangrove management trajectory is a more consequential determinant of coastal flood exposure than the choice of emissions scenario, a finding with direct implications for the prioritisation of coastal adaptation investment in Sabah and Sarawak.

The remainder of the paper is structured as follows. Section 2 describes the physical and ecological setting of the study area. Section 3 presents the datasets and analytical methods. Section 4 reports the results across the four analytical components: mangrove loss patterns, inundation zone extent, flood exposure change and population exposure, together with the forward-looking scenario matrix. Section 5 discusses the findings in the context of the existing literature and addresses the principal methodological limitations. Section 6 presents the conclusions and recommendations for future research.

## 2. Study Area

The study area encompasses the coastal zone of East Malaysia, comprising the states of Sabah and Sarawak, situated on the northwestern and northern portions of the island of Borneo (Figure 1). Together, the two states cover a combined land area of approximately 198,160 km², spanning from approximately 109.5°E to 119.3°E in longitude and from 0.85°N to 7.4°N in latitude. East Malaysia shares land borders with the Indonesian province of Kalimantan to the south and east, and surrounds the Sultanate of Brunei on Sarawak's northern coast. The study domain was defined as a 10 km inland coastal buffer delineated from the combined state boundary, encompassing approximately 49,655 km² of the coastal zone.

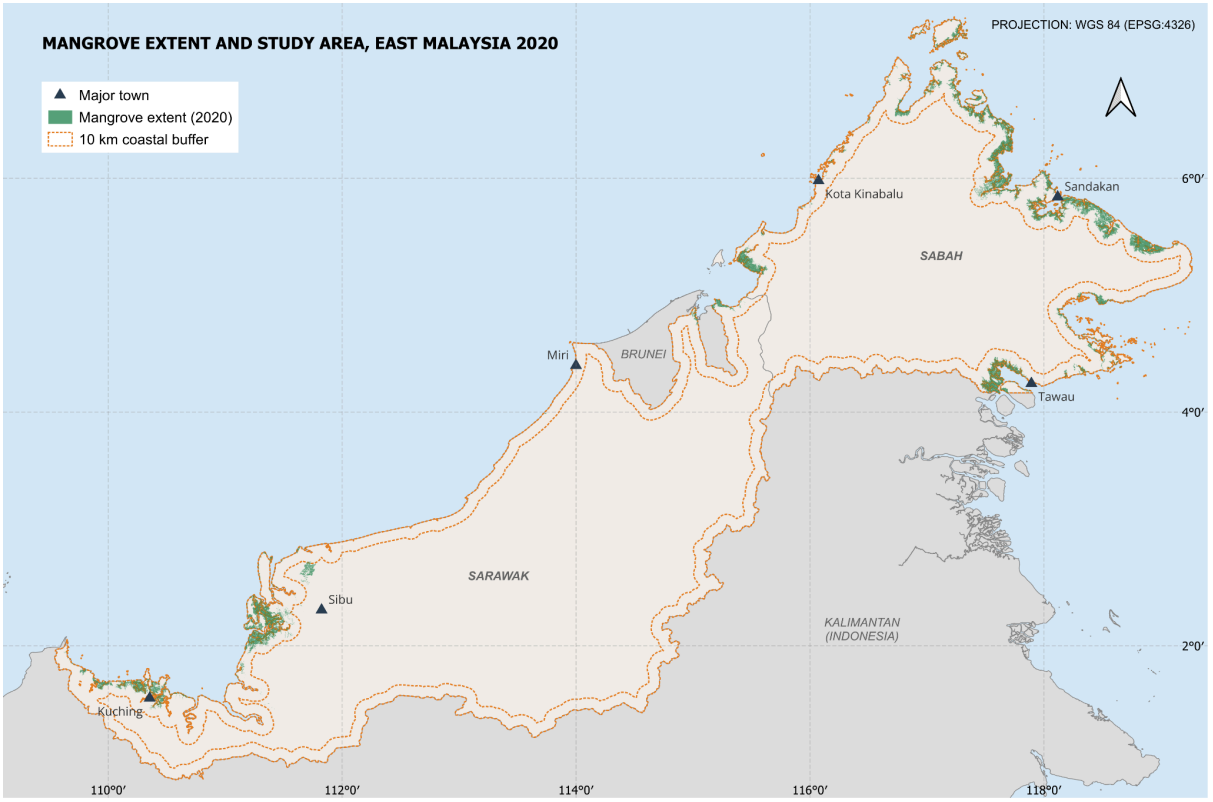


***Figure 1**. Overview map of the study area, showing the 10 km coastal buffer, state boundaries (Sabah and Sarawak), major coastal towns, and GMW v3.0 mangrove extent (2020). Projection: WGS 84 (EPSG:4326).*

Sarawak occupies the southwestern portion of the study area, with a coastline of approximately 1,050 km facing the South China Sea. The state is characterised by deeply incised river systems draining from the mountainous interior across broad coastal plains. The most ecologically and geomorphologically significant coastal feature is the Rajang Delta, the largest delta system in Malaysia and one of the largest in Southeast Asia, which debouches into the South China Sea near Sibu and Mukah. The delta supports extensive mangrove forests across its intertidal margins, interspersed with peat swamp forest and areas of active agricultural and aquaculture conversion. Other major river systems including the Baram, Trusan and Limbang also support mangrove-fringed estuarine environments along the northern Sarawak coast.

Sabah occupies the northeastern portion of the study area, with a more complex coastline facing the South China Sea to the west, the Sulu Sea to the northeast and the Celebes Sea to the east. The state's coastal geography is dominated in the east by the Kinabatangan floodplain and estuary, one of the most ecologically significant lowland river systems in Borneo, and by the sheltered bays and archipelagos of the Sandakan area, which support some of the most extensive remaining mangrove stands in Malaysia. The west coast is characterised by lower-lying coastal plains with scattered mangrove fringing.

The climate of East Malaysia is equatorial, with high year-round temperatures, elevated humidity and annual rainfall typically ranging from 2,500 to 4,000 mm, higher in interior upland areas. The coastline is subject to two monsoon seasons: the Southwest Monsoon (May to September) and the Northeast Monsoon (November to March), the latter bringing stronger winds and larger wave heights particularly along north- and east-facing coasts. Tropical cyclones are relatively infrequent in the South China Sea compared with the western Pacific, but the region is not immune to typhoon-induced storm surges, as demonstrated by the impacts of Typhoon Vamei (2001) and more localised extreme rainfall and surge events affecting the Sandakan and Tawau coastal zones. IBTrACS (International Best Track Archive for Climate Stewardship) records indicate that the East Malaysia coastline has been affected by multiple Category 1 to 2 equivalent systems since 1996 [7], with storm surges of 0.5 to 1.5 m documented in the Sandakan and Tawau areas of eastern Sabah. This range corresponds

directly to the inundation thresholds modelled in this study, providing empirical grounding for the chosen threshold envelope and underscoring the relevance of near-term coastal flood exposure quantification in the region.

East Malaysia holds approximately 82% of Malaysia's national mangrove extent, estimated at approximately 586,000 ha nationally [4]. Within the study area, the 2020 GMW v3.0 dataset records approximately 4,003 km² of mangrove within the 10 km coastal buffer. Sabah's mangroves are concentrated predominantly along the east coast, particularly in the Sandakan-Kinabatangan lowlands and Darvel Bay. Sarawak's mangroves are most extensive at the mouths of the major river systems, notably the Rajang Delta, and along the river mouths of the Baram and Limbang in the north.

The coastal lowlands of Sabah and Sarawak, particularly the deltaic and estuarine plains, are characterised by very low relief. Large areas of the Rajang Delta and the Kinabatangan floodplain lie at or below 2 m above mean sea level, rendering them inherently susceptible to tidal inundation and, under projected sea level rise, to permanent or chronic coastal flooding. These low-lying areas support a mixture of land uses including smallholder agriculture, oil palm plantations, aquaculture ponds and rural settlements, as well as remnant peat swamp and mangrove forest. The major coastal urban centres of Kuching (Sarawak's state capital), Sibu, Miri and Bintulu in Sarawak, and Kota Kinabalu (Sabah's state capital), Sandakan, Tawau and Lahad Datu in Sabah, are located in or adjacent to coastal lowland areas and concentrate the majority of the region's coastal population.

The regulatory framework governing mangrove forests in East Malaysia is administered primarily at the state level, with the majority of mangrove areas gazetted as Permanent Forest Reserves under the respective state forestry ordinances. However, mangroves on state land outside gazetted reserves, and those subject to de-gazettement for development purposes, remain vulnerable to clearance. Documented loss events in both the Rajang Delta and the Sandakan-Kinabatangan zone indicate that legal protection alone has not been sufficient to prevent mangrove conversion in some areas [18].

## 3. Data and Methods

### 3.1 Data Sources

Five publicly available datasets were used in this study. Table 1 provides a summary of each dataset, its source and its role in the analysis.

***Table 1***. *Summary of datasets used in this study.*

| Dataset | Source & Access | Spatial Resolution | Temporal Coverage | Role in Study |
|---|---|---|---|---|
| Global Mangrove Watch (GMW) v3.0 | Japan Aerospace Exploration Agency (JAXA) / Global Mangrove Alliance. Accessed via gmw.wetlands.org [12] | ~25 m (SAR-derived vector polygons) | 1996, 2007-2010, 2015-2020 (11 epochs) | Mangrove extent mapping; loss and gain quantification |
| GADM Administrative Boundaries v4.1 | University of California Davis. Accessed via gadm.org [8] | Vector polygons (administrative units) | Current (2023 release) | Study area delineation; Sabah and Sarawak boundary extraction |
| Copernicus DEM GLO-30 | European Space Agency / Copernicus Programme. AWS Open Data Registry (copernicus-dem-30m) [9] | ~30 m (1 arc-second) | 2011–2015 acquisition baseline | Inundation zone modelling; bathtub model elevation inputs |

| | | | | |
|---|---|---|---|---|
| WorldPop UN-adjusted Population Count (100 m) | WorldPop, University of Southampton (worldpop.org) [10] | 100 m | 2020 | Population exposure estimation within inundation zones |
| IPCC AR6 Regional Sea Level Rise Projections | NASA Sea Level Projection Tool (sealevel.nasa.gov/ipcc-ar6-sea-level-projection-tool) [13], based on Fox-Kemper et al. [11] | Point estimates at Bintulu (Sarawak) and Kota Kinabalu (Sabah) | Projections to 2050 and 2100 | Sea level rise scenario inputs; inundation threshold calibration |

#### 3.1.1 Global Mangrove Watch (GMW) v3.0

Mangrove extent data were sourced from the Global Mangrove Watch (GMW) version 3.0 dataset [12], produced by the Japan Aerospace Exploration Agency (JAXA) in collaboration with the Global Mangrove Alliance. GMW v3.0 provides annual vector polygon maps of global mangrove extent for 1996 and 2007 to 2020, derived from L-band Synthetic Aperture Radar (SAR) imagery integrated with optical data. Eleven annual layers were downloaded for the years 1996, 2007, 2008, 2009, 2010, 2015, 2016, 2017, 2018, 2019 and 2020, and clipped to the 10 km coastal buffer. The 2007 epoch is known to exhibit a slight upward artefact in extent estimates attributable to differences in SAR acquisition conditions; this is noted where relevant in the Results.

#### 3.1.2 Copernicus DEM GLO-30

Elevation data were sourced from the Copernicus Digital Elevation Model at 30 m resolution (GLO-30), accessed via the AWS Open Data Registry [9]. The GLO-30 DEM is derived from TanDEM-X radar interferometry acquisitions and represents the Earth's surface including vegetation and built structures (a digital surface model). A total of 47 tiles covering the Sabah and Sarawak coastal zone were downloaded, mosaicked and clipped to the study area. Ocean areas are encoded as NoData (-9999) in the GLO-30 product. The GLO-30 DEM uses EGM2008 (EPSG:3855) as its vertical reference datum, which approximates mean sea level globally but does not correspond to local tidal datums. For the East Malaysia coast, mean higher high water (MHHW) sits approximately 0.6 to 1.0 m above mean sea level depending on location, reflecting the mixed diurnal-semidiurnal tidal regime of the South China Sea and Sulu Sea. The inundation thresholds applied in this study (0.20 m to 1.50 m above the EGM2008 surface) therefore correspond approximately to the range between mean sea level and mean higher high water across the study area. This introduces a conservative bias at the lower thresholds: the directional effect is to slightly underestimate inundation extent at 0.20 m and 0.25 m, whilst the 1.00 m and 1.50 m thresholds are less sensitive to this offset. It is further acknowledged that the GLO-30 DEM represents surface elevation rather than bare-earth terrain elevation, and as such may overestimate ground elevation in vegetated areas, including mangroves, potentially causing a conservative underestimate of inundation extent. Both limitations are discussed further in Section 5.

#### 3.1.3 WorldPop Population Data

Population distribution data were obtained from the WorldPop UN-adjusted gridded population count for Malaysia (2020) at 100 m resolution [10]. The UN-adjusted product scales modelled population estimates to match official United Nations national population totals, providing greater comparability across countries. The raster was reprojected to match the inundation model grid (EPSG:4326, approximately 31 m) using bilinear resampling. Bilinear resampling onto a finer grid inflates raw pixel sums, as pixel values are interpolated across a larger number of output cells whilst preserving the spatial distribution of the original data. All reported population figures were therefore rescaled by a correction factor (0.535) derived from the ratio of the UN-adjusted Malaysian national total (32.9 million) to the reprojected raster sum, to restore internal consistency with official population estimates. Whilst mass-preserving zonal statistics on the native 100 m grid represent an alternative approach, the correction factor method produces figures anchored directly to the UN-adjusted national total and is considered sufficiently robust for the relative comparisons central to this study. The correction factor is applied uniformly across all inundation zones and population sub-categories, preserving the

internal proportionality of all reported exposure figures. It is acknowledged that bilinear interpolation inherently smooths local population density across cell boundaries; however, given the regional scale of this multi-decadal analysis, any localised edge-smoothing along the land-sea interface is expected to have a negligible impact on the overarching trends and comparative scenario dynamics.

#### 3.1.4 IPCC AR6 Sea Level Rise Projections

Regional sea level rise projections were extracted from the NASA IPCC AR6 Sea Level Projection Tool [13], based on the assessment of Fox-Kemper et al. [10] in IPCC AR6 Working Group I Chapter 9. Regional median values were obtained at two representative locations: Bintulu (Sarawak) and Kota Kinabalu (Sabah), capturing the longitudinal extent of the study area. Both locations yielded consistent regional median projections. Values are expressed relative to the 1995 to 2014 baseline. Two emissions scenarios were used: SSP2-4.5 (intermediate forcing) and SSP5-8.5 (high-end forcing), at the 2050 and 2100 time horizons (Table 2).

***Table 2**. IPCC AR6 regional sea level rise projections for East Malaysia (median values, relative to 1995–2014 baseline) [11, 13].*

| Scenario | 2050 Median (m) | 2100 Median (m) | Note |
|---|---|---|---|
| SSP2-4.5 | 0.20 | 0.56 | Regional value exceeds global mean (0.51 m) at 2100 owing to South China Sea ocean dynamics |
| SSP5-8.5 | 0.23 | 0.78 | — |

### 3.2 Analytical Methods

All analysis was conducted in Python using the geopandas, rasterio, pandas, numpy, scipy, seaborn and matplotlib libraries. QGIS was used for cartographic production of Figure 1 and visual inspection; no analytical operations were performed in QGIS. All spatial operations were performed in the projected coordinate reference system EPSG:32650 (WGS 84 / UTM Zone 50N) unless otherwise stated, with EPSG:4326 used where raster grid alignment required geographic coordinates. All data and analysis code supporting this study are openly available on Zenodo at https://doi.org/10.5281/zenodo.20620479.

#### 3.2.1 Study Area Delineation

The study area boundary was derived from the GADM v4.1 administrative polygon for Sabah and Sarawak combined. The two state polygons were dissolved into a single land polygon, from which a 10 km inland coastal buffer was generated and intersected with the land polygon to exclude ocean areas. The resulting study area polygon was saved as a GeoPackage and used as the spatial mask for all subsequent operations.

#### 3.2.2 Mangrove Extent and Loss Quantification

For each of the eleven GMW v3.0 epochs, mangrove polygons were clipped to the study area buffer and reprojected to EPSG:32650. Mangrove extent for each year was computed as the total polygon area in km². Net change was calculated as the difference between the 2020 and 1996 extents. Gross mangrove loss and gain over the full study period (1996 to 2020) were quantified using geometric difference overlays: loss polygons were derived as areas present in the 1996 layer but absent in the 2020 layer, and gain polygons as areas present in 2020 but absent in 1996. The gross loss area (114.06 km²) and gross gain area (67.72 km²) sum to the observed net change of -46.34 km². Loss hotspot analysis was conducted by aggregating gross loss polygon areas within a 0.1° × 0.1° grid, identifying spatial concentrations of mangrove loss across the coastline.

#### 3.2.3 Inundation Zone Modelling

Coastal inundation zones were modelled using a static bathtub approach with hydrological connectivity, applied to the Copernicus GLO-30 DEM at five elevation thresholds: 0.20 m, 0.25 m, 0.50 m, 1.00 m and 1.50 m above

current mean higher high water (MHHW). The 0.20 m and 0.25 m thresholds correspond to the IPCC AR6 regional median SLR projections for SSP2-4.5 and SSP5-8.5 at 2050, respectively. The 0.50 m, 1.00 m and 1.50 m thresholds represent the primary SLR scenarios for the retrospective exposure analysis.

The bathtub model identifies all DEM cells at or below each threshold elevation as candidate inundation cells. The EGM2008 geoid, which approximates mean sea level globally, is treated as the zero datum throughout; all inundation thresholds are therefore expressed as metres above mean sea level as represented by the EGM2008 surface. The land-sea interface in the model is defined by the NoData boundary in the GLO-30 product, where ocean pixels are encoded as NoData (-9999); this boundary corresponds to the satellite-derived land-water interface at the time of TanDEM-X acquisition rather than to a specific tidal datum. It is acknowledged that along the East Malaysia coast, mean higher high water (MHHW) sits approximately 0.6 to 1.0 m above mean sea level, meaning that the 0.20 m and 0.25 m thresholds applied in this study are structurally below the daily high tide line. These lower thresholds should therefore be interpreted as representing areas susceptible to inundation under modest SLR above the current mean sea level surface, rather than as areas currently experiencing tidal inundation. The 0.50 m, 1.00 m and 1.50 m thresholds are less sensitive to this datum offset and better approximate meaningful inundation boundaries in the context of local tidal ranges. A hydrological connectivity filter was then applied to remove isolated inland depressions that, despite meeting the elevation criterion, have no physical pathway to coastal floodwaters. Connectivity was determined using an 8-connected component labelling algorithm (scipy.ndimage.label). Sea seed pixels, defined as NoData (ocean) pixels spatially adjacent to valid land cells along the land-ocean interface, were used as the flood source. Only candidate cells belonging to connected components that intersected the sea seed layer were retained as inundated.

This connectivity filter substantially reduced the inundation extent compared to a naive elevation threshold: at the 1.50 m threshold, 17,726 total connected components were identified, of which only 235 were hydrologically connected to the sea; the remaining 17,491 isolated interior depressions were excluded. This approach provides a more physically realistic estimate of coastal flood exposure whilst remaining computationally tractable at regional scale. The inundation model does not account for wave setup, storm surge or dynamic flow processes, and is intended as a first-order estimate of areas susceptible to permanent or chronic inundation under the specified SLR scenarios. This limitation is discussed in Section 5.

### 3.2.4 Flood Exposure Change Analysis

Flood exposure attributable to mangrove loss was quantified by overlaying the inundation zone rasters with rasterised versions of the mangrove loss, gain and 2020 extent polygon layers. All vector layers were rasterised onto the inundation model grid prior to overlay using binary burn values. Pixel-level Boolean intersection identified: (i) inundated area coinciding with mangrove loss since 1996; (ii) inundated area coinciding with mangrove gain since 1996; and (iii) inundated area still protected by mangroves present in 2020. Population exposure within each zone was estimated by summing corrected WorldPop values within inundated pixels.

### 3.2.5 Forward-Looking Scenario Modelling

Future coastal flood exposure to 2050 was estimated through a scenario matrix combining projected mangrove loss trajectories with IPCC AR6 SLR projections. Three mangrove loss trajectories were constructed by fitting a linear regression to the observed 1996 to 2020 extent time series, excluding the 2007 epoch which is a known SAR acquisition artefact in the GMW v3.0 product (slope = -2.266 km²/year, $R^2 = 0.705$, $p = 0.002$) and extrapolating to 2050 at three rates:

- Low loss scenario: 50% of the observed trend rate (-1.13 km²/year), representing partial recovery or conservation intervention; projected additional loss 2020 to 2050: 34.0 km².
- Mid loss scenario: 100% of the observed trend rate (-2.27 km²/year), representing continuation of the historical trajectory; projected additional loss: 68.0 km².
- High loss scenario: 150% of the observed trend rate (-3.40 km²/year), representing accelerated loss under intensified land-use pressure; projected additional loss: 102.0 km².

These three mangrove trajectories were combined with the two IPCC AR6 SLR scenarios (SSP2-4.5 and SSP5-8.5 at 2050), producing a 3 by 2 scenario matrix of six future exposure estimates. Projected inundation areas at each SLR value were obtained by linear interpolation across the five modelled threshold brackets (0.20 m, 0.25 m, 0.50 m, 1.00 m and 1.50 m). Additional flood exposure attributable to projected mangrove loss was estimated using the empirically derived ratio of exposed area per unit of mangrove loss (0.42 km² of flood exposure per km² of mangrove lost), derived from the 1996 to 2020 retrospective analysis at the 1.0 m threshold. Population exposure in 2050 was projected by applying the observed population density within current inundation zones to the additional exposed area. The linear extrapolation of mangrove loss and the constant loss-to-exposure ratio are simplifying assumptions that do not capture nonlinear dynamics such as accelerating loss under climate feedbacks or landscape fragmentation thresholds. The forward-looking scenarios are therefore presented as indicative projections rather than predictions.

## 4. Results

### 4.1 Mangrove Loss Patterns and Rates, 1996–2020

Mangrove extent within the 10 km coastal buffer of East Malaysia declined from 4,049.35 km² in 1996 to 4,003.01 km² in 2020, a net loss of 46.34 km² (-1.14%) over the 24-year study period (Table 3). This rate of loss is modest relative to regional Southeast Asian averages, where annual losses of 0.18 to 0.28% per year have been reported [14, 18], and is consistent with the comparatively robust regulatory frameworks governing forestry in Sabah and Sarawak.

***Table 3***. *Mangrove extent within the 10 km coastal buffer of East Malaysia, 1996–2020. Values are in km², projected in EPSG:32650 (UTM Zone 50N). Changes are relative to the 1996 baseline.*

| Year | Extent (km²) | Change from 1996 (km²) | Notes |
|---|---|---|---|
| 1996 | 4,049.35 | — | Baseline |
| 2007 | 4,059.19 | +9.84 | Apparent gain — GMW SAR acquisition artefact (see text) |
| 2008 | 4,049.30 | −0.05 | — |
| 2009 | 4,049.25 | −0.10 | — |
| 2010 | 4,043.08 | −6.27 | — |
| 2015 | 4,022.21 | −27.14 | Steepest loss phase begins |
| 2016 | 4,006.55 | −42.80 | — |
| 2017 | 4,006.20 | −43.15 | — |
| 2018 | 4,013.48 | −35.87 | Partial recovery |
| 2019 | 4,016.70 | −32.65 | — |
| 2020 | 4,003.01 | −46.34 | Lowest recorded extent in the study period |

Three distinct temporal phases are evident in the time series (Figure 2). During the first phase (1996 to 2009), mangrove extent remained broadly stable, fluctuating within 10 km² of the 1996 baseline. The 2007 epoch shows an apparent uptick of +9.84 km² relative to 1996, which is attributable to a known systematic offset in SAR acquisition conditions in the GMW v3.0 product for that year rather than genuine mangrove gain [12]; this artefact has been noted by other studies using the GMW dataset and is treated as such here.

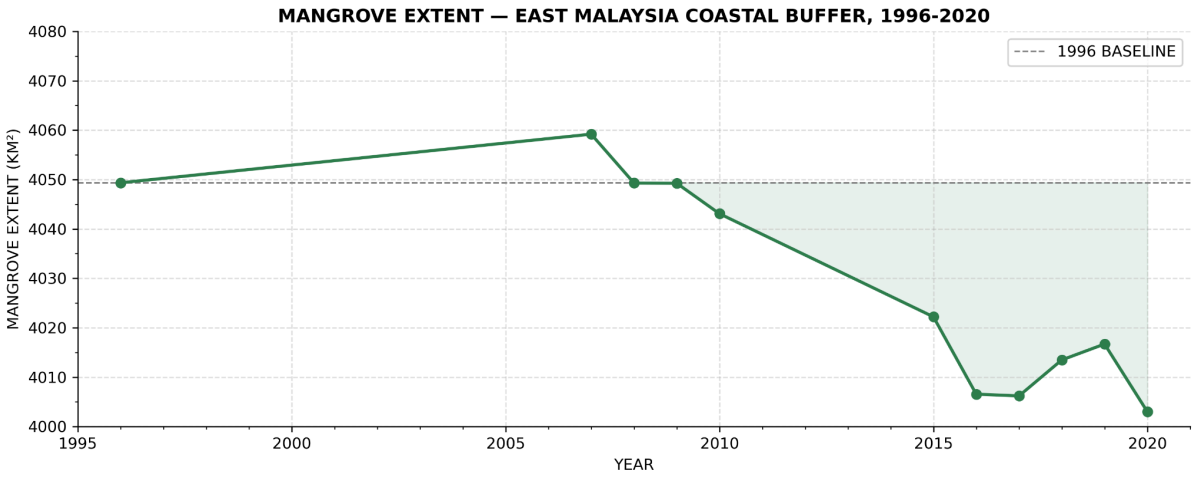


***Figure 2**. Mangrove extent within the 10 km coastal buffer of East Malaysia, 1996 to 2020, derived from the Global Mangrove Watch (GMW) v3.0 dataset [12]. The dashed line denotes the 1996 baseline extent (4,049.35 km²). The 2007 apparent uptick is attributable to a known SAR acquisition artefact in the GMW v3.0 product rather than genuine mangrove gain. The shaded area beneath the curve illustrates cumulative departure from the baseline.*

The second phase (2010 to 2016) was characterised by accelerating loss, with extent declining by 36.53 km², representing more than three-quarters of the total net loss within just six years. This period coincides with intensification of oil palm expansion into coastal and peat-swamp areas in both states, as well as expansion of coastal aquaculture [18]. The third phase (2017 to 2019) shows a partial recovery of 10.50 km², likely reflecting natural regeneration and reduced clearing pressure, before the extent declined again to its lowest recorded value of 4,003.01 km² in 2020.

Gross loss and gain calculations reveal a more dynamic landscape than the net figure suggests. Over the full 1996 to 2020 period, 114.06 km² of mangrove was lost whilst 67.72 km² of new cover was recorded in 2020 in areas not mapped in 1996. This gross loss figure is approximately 2.5 times greater than the net change, underscoring the importance of reporting both metrics [16].

Spatial analysis of gross loss polygons using a 0.1° × 0.1° grid identified four principal hotspot regions across the East Malaysia coastal buffer (Table 4; Figure 3). The dominant loss signal originates from Hotspot A (Rajang Delta), where the highest-ranked cell (lon 111.2°E, lat 2.6°N) recorded a gross loss of 11.21 km², the largest of any single cell across the study area. Three further Rajang Delta cells rank within the top ten nationally, confirming this delta system as the primary locus of mangrove loss in East Malaysia, consistent with documented oil palm and aquaculture expansion in this zone [18].

***Table 4**. Top ten gross mangrove loss hotspot cells (0.1° × 0.1° grid), East Malaysia coastal buffer, 1996–2020. Four named hotspot regions are identified on the basis of geographic clustering. Cell coordinates refer to the south-west corner of each grid cell.*

| Rank | Longitude (°E) | Latitude (°N) | Gross Loss (km²) | Hotspot Region |
|---|---|---|---|---|
| 1 | 111.20 | 2.60 | 11.21 | A — Rajang Delta |
| 2 | 115.40 | 5.20 | 3.49 | C — Menumbok Forest Reserve |
| 3 | 111.30 | 2.20 | 3.25 | A — Rajang Delta |
| 4 | 110.40 | 1.60 | 2.84 | B — SW Sarawak coast |
| 5 | 110.30 | 1.60 | 2.61 | B — SW Sarawak coast |
| 6 | 119.00 | 5.30 | 2.59 | D — Kinabatangan coast |

| | | | | |
|---|---|---|---|---|
| 7 | 110.10 | 1.60 | 2.46 | B — SW Sarawak coast |
| 8 | 118.80 | 5.40 | 2.46 | D — Kinabatangan coast |
| 9 | 118.40 | 5.70 | 2.35 | D — Kinabatangan coast |
| 10 | 111.20 | 2.00 | 2.12 | A — Rajang Delta |

Hotspot B (SW Sarawak coast), south of Kuching, contributes three cells to the top ten (ranks 4, 5 and 7), with individual cell losses of 2.46 to 2.84 km², reflecting ongoing coastal and peatland conversion in the southwestern Sarawak lowlands. In Sabah, Hotspot C (Menumbok Forest Reserve) on the SW Sabah coast registers a top-ten cell loss of 3.49 km² (rank 2), representing a geographically concentrated loss signal within a formally designated forest reserve that warrants further investigation into the efficacy of existing protection in this area. Hotspot D (Kinabatangan coast) in northeastern Sabah contributes three cells to the top ten (ranks 6, 8 and 9), with individual losses of 2.35 to 2.59 km², consistent with the well-documented pattern of aquaculture and plantation expansion in the Sandakan-Kinabatangan lowlands [18]. The spatial distribution of all hotspot cells is shown in Figure 3, with a detailed zoom of Hotspot A provided in Figure 4.

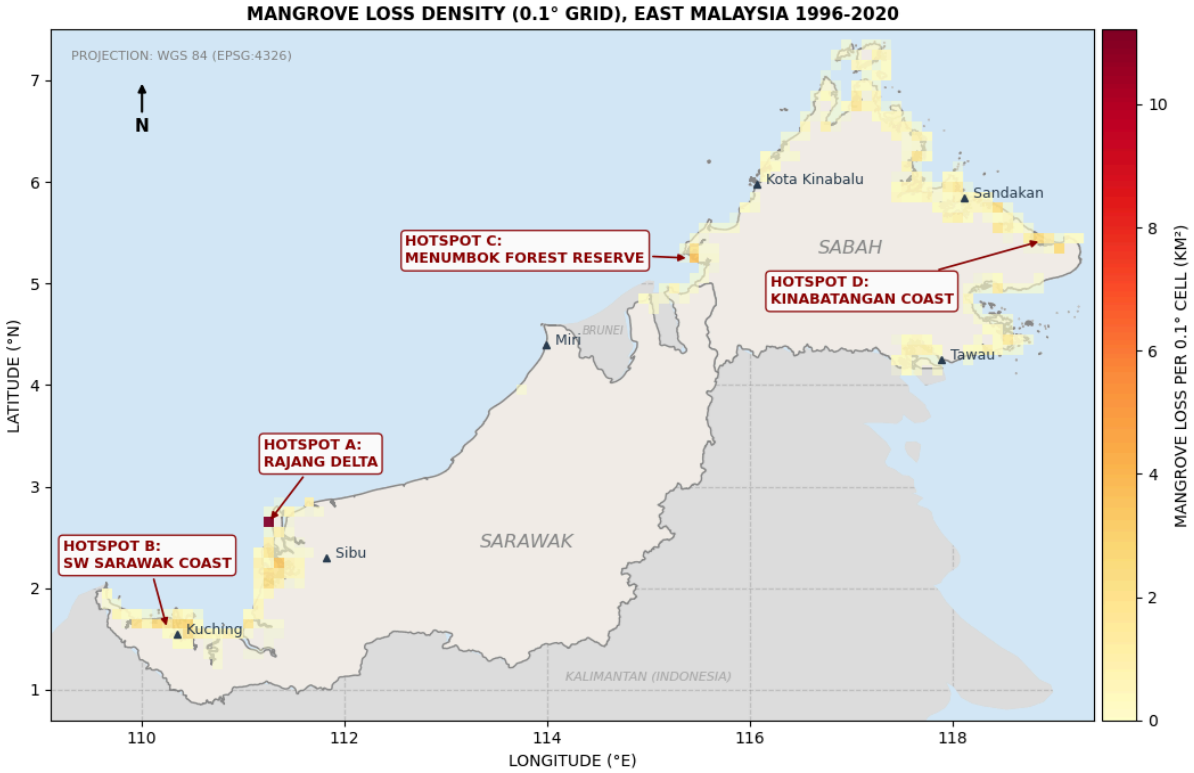


***Figure 3***. *Spatial distribution of gross mangrove loss density (0.1° × 0.1° grid) within the East Malaysia 10 km coastal buffer, 1996–2020. Grid cells are coloured by gross loss area (km²) on a yellow-orange-red scale. Four named hotspot regions are annotated: Hotspot A (Rajang Delta), Hotspot B (SW Sarawak coast), Hotspot C (Menumbok Forest Reserve) and Hotspot D (Kinabatangan coast). Major coastal towns are shown for geographic reference. Projection: WGS 84 (EPSG:4326).*

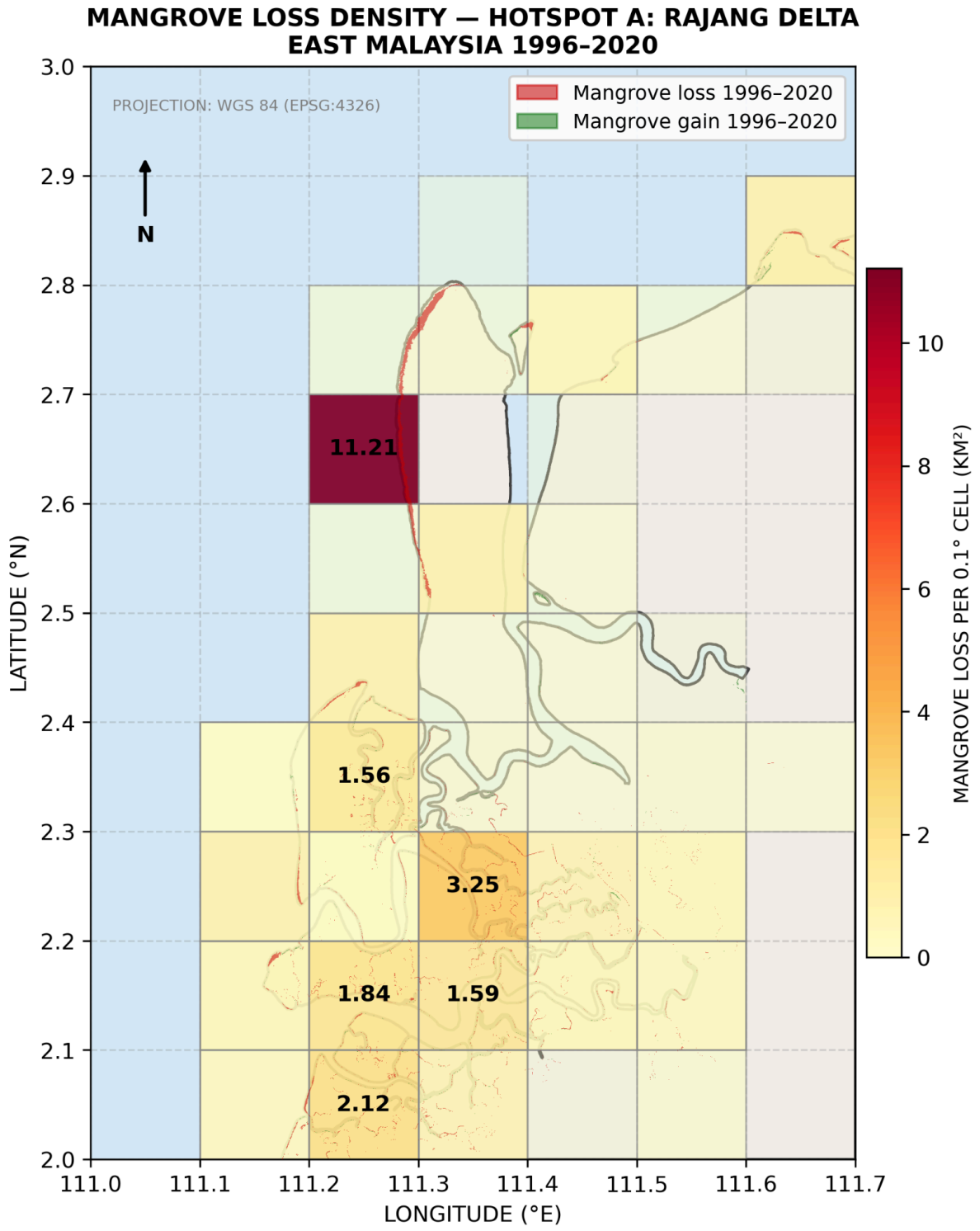


***Figure 4***. *Zoomed view of Hotspot A (Rajang Delta), showing gross mangrove loss polygons (red) and gain polygons (green) overlaid on the 0.1° loss density grid, 1996–2020. Grid cell values (km²) are shown for cells with gross loss ≥ 1.0 km². Projection: WGS 84 (EPSG:4326).*

### 4.2 Inundation Zone Extent Under Sea Level Rise Thresholds

Application of the hydrologically-connected bathtub model to the Copernicus GLO-30 DEM produced inundation zone estimates at five elevation thresholds (Table 5). At the SLR-relevant thresholds of 0.20 m and 0.25 m, corresponding to the IPCC AR6 regional median projections for SSP2-4.5 and SSP5-8.5 at 2050

respectively, inundation zones of 526.4 km² and 528.4 km² were identified. At the three primary analytical thresholds of 0.50 m, 1.00 m and 1.50 m, inundation zones expand progressively to 618.9 km², 712.7 km² and 806.1 km².

***Table 5**. Hydrologically-connected inundation zone extent at five elevation thresholds, East Malaysia 10 km coastal buffer. All areas in km².*

| Threshold (m) | Inundation Area (km²) | Notes |
|---|---|---|
| 0.20 | 526.4 | SSP2-4.5 2050 regional median SLR |
| 0.25 | 528.4 | SSP5-8.5 2050 regional median SLR (interpolated) |
| 0.50 | 618.9 | Primary analytical threshold |
| 1.00 | 712.7 | Primary analytical threshold |
| 1.50 | 806.1 | Primary analytical threshold |

The relatively modest increment between the 0.20 m and 0.50 m thresholds (+92.5 km², +17.6%) compared with the 0.50 m to 1.50 m increment (+187.2 km², +30.2%) reflects the low-gradient character of the East Malaysian coastal lowlands, where much of the immediately coastal terrain lies below 0.5 m, with a gradual transition to slightly higher ground further inland within the buffer. The connectivity filter was essential to the physical validity of the inundation estimates. At the 1.50 m threshold, only 235 of 17,726 connected components (1.3%) were hydrologically connected to the open ocean; the remaining 17,491 isolated interior depressions were excluded, which would otherwise have substantially inflated the inundation estimate.

### 4.3 Flood Exposure Change Attributable to Mangrove Loss

Overlay of the inundation zone rasters with the mangrove loss and 2020 extent layers reveals the spatial extent to which mangrove loss since 1996 has increased the area directly exposed to potential inundation (Table 6). At the 0.50 m threshold, 43.79 km² of the 618.9 km² inundation zone (7.1%) falls within areas that had mangrove cover in 1996 but lost it by 2020 — coastal lowland areas that previously benefited from biophysical buffering [15] but no longer do so. This figure rises to 48.10 km² (6.7%) at 1.00 m and 52.14 km² (6.5%) at 1.50 m.

***Table 6**. Flood exposure attributable to mangrove loss and gain, East Malaysia coastal buffer. 'Flooded via mangrove loss' denotes inundation zone area coinciding with land that lost mangrove cover between 1996 and 2020. 'Still protected' denotes inundation zone area with mangrove cover present in 2020. 'Unprotected fraction' is the proportion of the total inundation zone coinciding with mangrove loss areas.*

| SLR Threshold (m) | Total Inundation Zone (km²) | Flooded via Mangrove Loss (km²) | Flooded via Mangrove Gain (km²) | Still Protected by Mangroves (km²) | Unprotected Fraction (%) |
|---|---|---|---|---|---|
| 0.50 | 618.9 | 43.79 | 8.07 | 72.16 | 7.1% |
| 1.00 | 712.7 | 48.10 | 9.14 | 85.10 | 6.7% |
| 1.50 | 806.1 | 52.14 | 9.97 | 101.88 | 6.5% |

The marginal decrease in the unprotected fraction with increasing threshold (7.1% to 6.5%) reflects the spatial geometry of the system: mangrove loss has been concentrated at the immediate coastal fringe, already within the lowest inundation threshold, whilst additional land exposed at higher thresholds lies somewhat further inland.

A further 72.16 to 101.88 km² of the inundation zone retains active mangrove cover as of 2020, continuing to provide biophysical coastal protection to an estimated 32,600 to 51,400 people. The continued integrity of this buffer underscores the conservation value of the surviving mangrove stock. Mangrove gain areas (8.07 to 9.97 km²) contribute a modest but non-negligible offset, with new growth colonising some low-lying areas that would otherwise lie unprotected within the inundation zone.

## 4.4 Population Exposure

Population within the inundation zones was estimated by overlaying the WorldPop 2020 UN-adjusted gridded population dataset with the inundation zone rasters (Table 7). All figures have been corrected for resampling-induced inflation (correction factor: 0.535; see Section 3.1.3).

***Table** 7. Estimated population exposure within inundation zones, East Malaysia coastal buffer, 2020. Figures are corrected WorldPop UN-adjusted estimates (correction factor 0.535 applied; see Section 3.1.3). Tilde (~) denotes approximate values given raster resolution and resampling uncertainties.*

| SLR Threshold (m) | Total Population Exposed | Population in Former Mangrove Zone | Population Still Behind Mangroves |
|---|---|---|---|
| 0.50 | ~285,600 | ~10,200 | ~32,600 |
| 1.00 | ~341,100 | ~11,380 | ~40,900 |
| 1.50 | ~417,300 | ~12,730 | ~51,400 |

At the 0.50 m threshold, approximately 285,600 people currently reside within the modelled inundation zone. Of these, approximately 10,200 live in areas where mangrove cover was present in 1996 but has since been lost, representing a population now exposed to coastal inundation risk that previously benefited from a degree of natural buffering from mangrove ecosystems [15]. A further approximately 32,600 people remain landward of surviving 2020 mangrove stands and continue to benefit from their protective function.

Population exposure scales with inundation threshold, reaching approximately 341,100 at 1.00 m and 417,300 at 1.50 m. The population in the former mangrove zone increases consistently from approximately 10,200 to 12,730 across the threshold range, confirming that mangrove loss has exposed a non-trivial number of coastal residents to heightened flood risk.

The spatial pattern of exposure is concentrated around the major coastal urban centres and river deltas of East Malaysia. Coastal settlements in the Kuching Division and around the Rajang Delta (Sarawak), and the Sandakan-Kinabatangan lowlands (Sabah), account for the majority of exposed population, consistent with the four hotspot regions identified in Section 4.1 and illustrated in Figures 3 and 4.

## 4.5 Forward-Looking Scenario Projections to 2050

The retrospective analysis in Sections 4.1 to 4.4 establishes the degree to which mangrove loss between 1996 and 2020 has already increased coastal flood exposure in East Malaysia. This section extends the analysis forward to 2050 by combining projected mangrove loss trajectories with the IPCC AR6 regional sea level rise projections for SSP2-4.5 and SSP5-8.5, producing a scenario matrix of six plausible futures.

### 4.5.1 Projected Mangrove Loss Trajectories

A linear regression fitted to the observed 1996 to 2020 mangrove extent time series, excluding the 2007 SAR artefact epoch, yields a trend of -2.266 km² per year ($R^2 = 0.705$, $p = 0.002$), indicating a statistically significant and sustained decline over the study period. Excluding the artefact epoch marginally steepens the $R^2$ whilst modestly reducing the absolute slope, confirming that inclusion of the 2007 anomaly had introduced a slight conservative bias in the original trend estimate. Whilst the observed time series exhibits nonlinear phases, as documented in Section 4.1, the linear trend captures the central tendency of the loss trajectory and provides a defensible basis for near-term extrapolation to 2050.

Three trajectories were constructed by scaling the observed trend rate (Table 8). The low loss trajectory (-1.24 km²/year, 50% of the observed rate) represents partial recovery or conservation intervention, yielding 37.1 km² of additional loss by 2050. The mid loss trajectory (-2.48 km²/year, 100% of trend) assumes continuation of the historical trend, yielding 74.3 km². The high loss trajectory (-3.71 km²/year, 150% of trend) represents accelerated loss under intensified land-use pressure, yielding 111.4 km² of additional loss by 2050.

***Table 8**. Projected mangrove loss trajectories for East Malaysia, 2020 to 2050. Annual rates are derived from the observed 1996 to 2020 linear trend (slope = -2.266 km²/year, $R^2$ = 0.705, p = 0.002). Projected extents are relative to the 2020 baseline of 4,003.01 km².*

| Scenario | Annual Rate (km²/yr) | Additional Loss 2020-2050 (km²) | Projected 2050 Extent (km²) | Basis |
|---|---|---|---|---|
| Low loss | -1.13 | 34.0 | 3,969.0 | 50% of observed trend; conservation intervention or partial recovery |
| Mid loss | -2.27 | 68.0 | 3,935.0 | 100% of observed trend; continuation of historical trajectory |
| High loss | -3.40 | 102.0 | 3,901.0 | 150% of observed trend; accelerated loss under intensified land-use pressure |

It should be noted that the linear extrapolation assumes a constant rate of loss and does not capture potential nonlinear dynamics, including threshold effects arising from landscape fragmentation, climate-driven dieback or sudden policy shifts. The three trajectories are therefore presented as indicative scenario bounds rather than probabilistic forecasts, and should be interpreted accordingly.

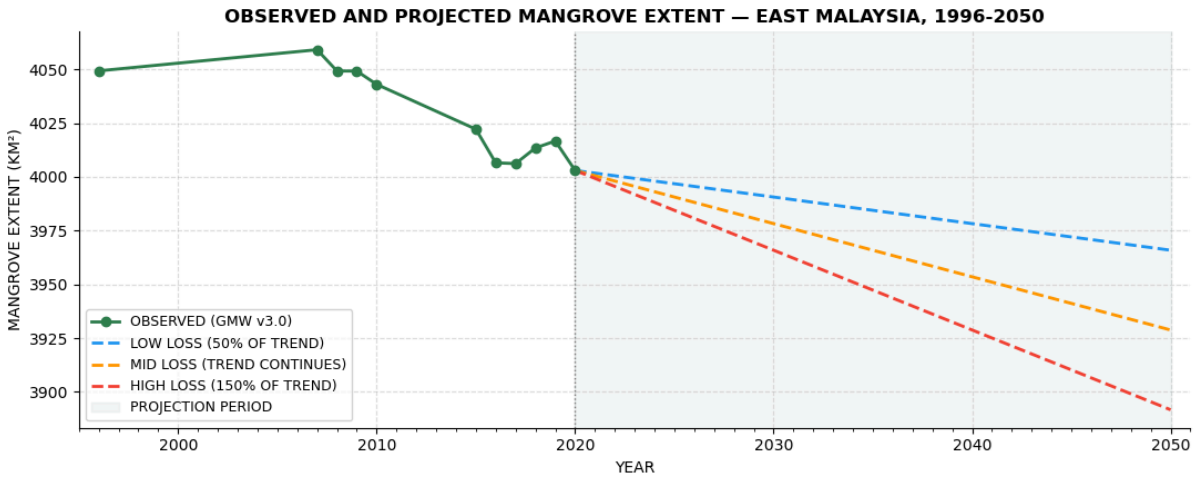


***Figure 5**. Observed mangrove extent within the East Malaysia 10 km coastal buffer (1996 to 2020, GMW v3.0) and projected extent to 2050 under low, mid and high loss scenarios. The vertical dashed line at 2020 denotes the boundary between the observational record and the projection period.*

### 4.5.2 Scenario Matrix: Combined SLR and Mangrove Loss Projections

The six scenario combinations are presented in Table 9. For each combination, the base inundation area reflects the hydrologically-connected zone at the 2050 IPCC AR6 median SLR threshold (0.20 m for SSP2-4.5 and 0.23 m for SSP5-8.5, interpolated from the modelled brackets). Additional flood exposure is estimated using the empirically derived loss-to-exposure ratio of 0.42 km² per km² of mangrove lost. Population exposure in 2050 is estimated by applying the current observed population density within the inundation zone to the additional exposed area.

***Table 9**. Scenario matrix of projected coastal flood exposure and population exposure in 2050, East Malaysia 10 km coastal buffer. Base inundation areas are interpolated from the hydrologically-connected bathtub model at the IPCC AR6 2050 median SLR values for each emissions scenario. Additional exposure is estimated using the observed loss-to-exposure ratio of 0.42 km² per km² of mangrove lost. Population figures are corrected WorldPop estimates (correction factor 0.535 applied; see Section 3.1.3).*

| SLR Scenario | Mangrove Scenario | Additional Mangrove Loss (km²) | Base Inundation (km²) | Additional Exposure (km²) | Total Exposure (km²) | Population Exposed (2050) |
|---|---|---|---|---|---|---|
| SSP2-4.5 | Low loss | 34.0 | 526.4 | 14.28 | 540.7 | 225,793 |
| SSP2-4.5 | Mid loss | 68.0 | 526.4 | 28.56 | 555.0 | 231,757 |
| SSP2-4.5 | High loss | 102.0 | 526.4 | 42.84 | 569.2 | 237,720 |
| SSP5-8.5 | Low loss | 34.0 | 527.6 | 14.28 | 541.9 | 226,295 |
| SSP5-8.5 | Mid loss | 68.0 | 527.6 | 28.56 | 556.2 | 232,258 |
| SSP5-8.5 | High loss | 102.0 | 527.6 | 42.84 | 570.4 | 238,222 |

#### 4.5.3 Implications for Coastal Flood Exposure and Population

Two findings of particular significance emerge from the scenario matrix. The spread attributable to mangrove loss scenario choice (approximately 28.6 km² between low and high loss within either SLR scenario) substantially exceeds the spread attributable to SLR scenario choice (approximately 1.2 km² between SSP2-4.5 and SSP5-8.5 within any given mangrove scenario). At the 2050 horizon, the trajectory of mangrove loss is therefore a more consequential determinant of coastal flood exposure than the choice of emissions scenario. This reflects the proximity of the 2050 time horizon: the regional SLR projections for SSP2-4.5 and SSP5-8.5 diverge substantially only beyond mid-century, whereas mangrove loss compounds continuously from the present day.

In terms of population exposure, the scenario matrix projects between approximately 225,800 and 238,200 people within the flood exposure zone by 2050. The difference of approximately 12,400 between best and worst case represents a number comparable in scale to the population of a small Malaysian coastal town, driven entirely by projected mangrove loss rather than by SLR scenario choice. These findings carry a clear policy implication: in East Malaysia, near-term investment in mangrove conservation and restoration has a greater measurable effect on 2050 coastal flood exposure than the difference between intermediate and high emissions pathways. Whilst long-term SLR trajectories beyond 2050 will eventually dominate the exposure picture under SSP5-8.5, the period to 2050 is one in which mangrove management decisions are the primary lever available to coastal risk managers. It is acknowledged that the scenario projections carry several sources of uncertainty. The loss-to-exposure ratio (0.42 km² per km²) assumes this spatial relationship remains stable under future conditions; changes in coastal geomorphology or the distribution of future loss could alter it. Similarly, the WorldPop-based projections do not account for future demographic change or coastal migration. These limitations are discussed further in Section 5.

## 5. Discussion and Limitations

### 5.1 Mangrove Loss in Regional Context

The net loss of 46.34 km² (1.14%) recorded across the East Malaysia coastal buffer between 1996 and 2020 is modest in absolute terms relative to other mangrove-holding nations in Southeast Asia, where losses have historically been more severe. Richards and Friess [18] reported a regional average annual loss rate of 0.18% per year across Southeast Asia between 2000 and 2012, driven primarily by aquaculture conversion and, in Malaysia and Indonesia specifically, by oil palm expansion. The annual equivalent of our observed net loss

(approximately 0.048% per year) falls well below this regional average, consistent with the comparatively strong formal protection afforded to East Malaysian mangroves through Permanent Forest Reserves, national parks and Ramsar designations. Approximately 85% of Malaysia's mangrove area is estimated to fall within such designated areas [12], which confers a meaningful degree of protection relative to less-regulated jurisdictions in the region.

However, the gross loss figure of 114.06 km² tells a more sobering story. The net figure is the outcome of substantial simultaneous loss and gain processes, and a net loss of only 46 km² masks the permanent removal of over 114 km² of mangrove from the coastal fringe. Goldberg et al. [16] emphasised that gross loss figures better capture the ecological disturbance associated with mangrove change, since newly gained mangrove in one location does not immediately replicate the structural complexity, biodiversity or protective function of mature mangrove lost elsewhere.

The Rajang Delta and Sandakan-Kinabatangan hotspots identified in this study are consistent with patterns documented for Malaysian Borneo more broadly, where oil palm expansion into peat-swamp and coastal zones has been identified as a key but underappreciated driver of mangrove loss [18]. The identification of Hotspot C (Menumbok Forest Reserve) in southwestern Sabah as the second-ranked loss cell nationally, with 3.49 km² of gross loss recorded within a formally designated Permanent Forest Reserve, raises a more specific concern: that legal designation alone has not been sufficient to prevent mangrove loss in this area, echoing the broader pattern noted by Richards and Friess [18] regarding the uneven effectiveness of protection across Malaysian Borneo. The mechanisms underlying this loss cannot be definitively established from remote sensing data alone; plausible drivers include unauthorised encroachment, incremental degazettement for aquaculture or coastal development purposes, or climate-driven dieback associated with altered hydrology in this low-lying coastal zone. Distinguishing between these drivers would require plot-level land-use change records and enforcement data beyond the scope of this study, and represents a priority for future investigation given the formal protected status of this area.

The loss hotspots identified in this study, particularly Hotspot A (Rajang Delta) and Hotspot B (SW Sarawak coast), coincide with areas of known coastal peat swamp overlap. The Rajang-Belawai Delta has been identified as holding significant blue carbon potential, with mangrove soils in peat-overlain coastal systems storing carbon stocks well in excess of mineral-soil mangroves. Mangrove conservation in these hotspot areas therefore carries a co-benefit beyond coastal flood protection: avoided carbon emissions from peat oxidation and disturbance, a dimension of direct relevance to emerging blue carbon market mechanisms and Malaysia’s national climate commitments. A comparison with the Indonesian portion of Borneo (Kalimantan) provides instructive regional context. Approximately 37% of Kalimantan’s original mangrove area has been lost, a figure substantially higher than the 1.14% net loss recorded for the East Malaysia coastal buffer in this study over 1996 to 2020. From 2000 to 2016, Indonesia experienced mangrove loss of approximately 3,363 km², with Kalimantan and Sulawesi identified as the primary hotspots of conversion [16], driven predominantly by aquaculture and oil palm expansion under weaker regulatory oversight than the Malaysian Permanent Forest Reserve system. Richards and Friess [18] estimated a Southeast Asia-wide average annual loss rate of 0.18% between 2000 and 2012; East Malaysia’s observed rate of approximately 0.05% per year over 1996 to 2020 sits well below this regional average, suggesting that the Permanent Forest Reserve framework has provided meaningful but incomplete protection. The persistence of loss within formally gazetted areas, most clearly illustrated by Hotspot C (Menumbok Forest Reserve), indicates that legal designation alone is insufficient without active enforcement and monitoring.

The three-phase temporal pattern observed in this study, comprising a stable period (1996 to 2009), a steep decline (2010 to 2016) and a partial recovery (2017 to 2019) before reaching a new low in 2020, warrants further investigation. The acceleration between 2010 and 2016 coincides broadly with intensified commodity-driven land-use change in Malaysian Borneo, though definitive causal attribution would require plot-level land-use change data beyond the scope of this study. Disentangling these drivers represents an important direction for future work.

## 5.2. Flood Exposure and the Role of Mangrove Loss

The finding that 43.79 to 52.14 km² of the modelled inundation zone across the three primary SLR thresholds formerly carried mangrove cover represents a quantifiable signal of loss-driven exposure increase. Whilst the unprotected fraction (6.5 to 7.1% of the total inundation zone) may appear modest in proportional terms, it represents a meaningful area of coastal lowland, encompassing an estimated 10,200 to 12,730 people, that has transitioned from a naturally buffered to an unprotected state within the study period.

The protective function of mangroves against coastal inundation operates through multiple mechanisms, including wave energy dissipation, storm surge attenuation and sediment trapping that maintains coastal elevation [15]. Van Wesenbeeck et al. [19] demonstrated through large-scale numerical modelling that mangrove forests wider than 500 m can dissipate approximately 75% of incoming wave energy, though narrower fringes, which characterise much of the East Malaysian coastal mangrove belt, provide more variable protection depending on local hydrodynamic conditions and forest density. The loss-to-exposure ratio derived in this study (0.42 km² of inundation zone per km² of mangrove lost) reflects the net spatial relationship between historical mangrove removal and inundation exposure, rather than the full hydrodynamic protective function, and should not be interpreted as a direct measure of wave attenuation or surge reduction.

The still-protected zone of 72.16 to 101.88 km² remaining behind 2020 mangrove stands is of particular significance from a conservation standpoint, providing coastal buffering to an estimated 32,600 to 51,400 people. Its continued integrity is therefore not merely an ecological concern but a direct determinant of coastal flood risk. Any further loss from this zone would translate directly into additional unprotected exposure at approximately 0.42 km² per km² of mangrove lost.

## 5.3. Scenario Projections and the Primacy of Mangrove Management

The scenario matrix confirms that at the 2050 horizon, mangrove loss trajectory is a more consequential determinant of coastal flood exposure than SLR emissions scenario choice, with the spread between low and high loss scenarios (~29 km², ~12,400 people) exceeding the SSP2-4.5 to SSP5-8.5 spread (~1.2 km², ~500 people) by more than an order of magnitude. This result reflects the convergence of the two IPCC AR6 SLR projections at 2050 (0.20 m vs 0.23 m regionally), with trajectories diverging substantially only in the second half of the century.

This finding does not diminish the importance of emissions mitigation. Beyond 2050, particularly under SSP5-8.5, regional SLR projections diverge considerably (0.56 m vs 0.78 m at 2100), producing inundation zones far larger than those modelled here. However, for coastal risk managers working within a near-term planning horizon, mangrove conservation and restoration represent the more immediately actionable lever on 2050 flood exposure, consistent with the broader literature on nature-based solutions [15].

The linear trend extrapolation used to construct the three mangrove loss trajectories necessarily simplifies a complex, nonlinear system. Should a loss acceleration similar to 2010 to 2016 recur, the high loss trajectory could prove optimistic. Conversely, operationalisation of Malaysian government commitments to no net forest loss at the coastal zone level could place outcomes below the low loss scenario. The scenario bounds should therefore be understood as plausible envelopes around an uncertain future rather than probabilistic estimates.

## 5.4 Limitations

Several methodological limitations of this study should be considered when interpreting the results.

1. **Inundation model**. The static bathtub model, even with hydrological connectivity, does not capture the dynamic processes governing real coastal flooding, including wave propagation, storm surge amplification, tidal variation, sediment transport or the spatial heterogeneity of flood duration and depth. Sanders et al. [20] have argued forcefully that bathtub modelling introduces systematic biases in

flood risk estimation and that physics-based approaches are now computationally feasible at regional scale. The inundation extents reported here should therefore be understood as indicative of areas susceptible to chronic inundation or permanent submergence under the specified SLR thresholds, rather than as predictions of discrete flood events. They provide a consistent relative basis for comparing exposure across thresholds and scenarios, which is the primary analytical purpose of this study. Additionally, the inundation thresholds are applied relative to the EGM2008 geoid rather than a local tidal datum. Given that MHHW exceeds mean sea level by approximately 0.6 to 1.0 m along the East Malaysia coast, the lower modelled thresholds (0.20 m and 0.25 m) should be interpreted as indicative of near-mean-sea-level exposure rather than tidal inundation frequency. Future work incorporating a local tidal datum correction would improve the physical interpretability of the lower threshold results.

2. **DEM quality**. The Copernicus GLO-30 is a digital surface model rather than a bare-earth digital terrain model, meaning that vegetation canopy and built structures are included in the elevation signal. In densely vegetated mangrove environments, mangrove canopies typically reach 10 to 25 m in height across the Indo-Pacific region, meaning the DEM may overestimate true ground elevation by a commensurate margin in mangrove-fringed areas, with a consequent conservative underestimation of inundation extent precisely in the coastal fringe zones most relevant to this study. The practical implication for the 2050 exposure metrics is that the reported inundation areas and population exposure figures should be regarded as lower-bound estimates in mangrove-fringed terrain: the true extent of flood-susceptible land in these zones is likely greater than modelled. This conservative bias is consistent across all six scenario combinations in Table 9 and does not affect the relative ordering of scenarios or the core finding that mangrove management trajectory dominates over SLR scenario choice at the 2050 horizon. Bare-earth LiDAR-derived DEMs or the CoastalDEM product (Climate Central) would substantially reduce this source of uncertainty, and should be considered in future work where data access permits.
3. **Population data**. The WorldPop gridded population estimates carry their own uncertainties, including the assumptions underlying the dasymetric modelling used to distribute population counts spatially. The bilinear resampling correction applied in this study addresses the most tractable source of inflation but does not resolve deeper uncertainties in the spatial allocation of population to low-lying coastal areas. Furthermore, the 2020 WorldPop baseline does not account for projected population growth, urbanisation or potential coastal migration by 2050, all of which could substantially alter the number of people at risk within the inundation zone.
4. **Mangrove protective function**. This study quantifies the spatial extent of the inundation zone formerly protected by mangroves, using a binary presence/absence framework. It does not model the hydrodynamic protective function of mangroves, which depends on forest width, density, species composition and the nature of the flood hazard (wave versus surge). The loss-to-exposure ratio (0.42 $km^2/km^2$) is an empirically derived spatial statistic rather than a physically based estimate of protective capacity, and should not be extrapolated beyond the specific geographic and hydrological context of this study.
5. **Scenario assumptions**. The forward-looking scenario matrix assumes a spatially and temporally constant relationship between mangrove loss and flood exposure, and a stable population density within the inundation zone. The scenario projections are best regarded as sensitivity analyses illustrating the relative importance of mangrove management versus SLR scenario choice, rather than as independent forecasts of 2050 exposure.

Despite these limitations, this study provides the first systematic quantification of loss-driven coastal flood exposure change for the East Malaysia coastline using freely available global datasets and a reproducible, open-source analytical workflow. The approach is transferable to other mangrove-holding coastlines in Southeast Asia and the broader Indo-Pacific, and the results provide a defensible evidence base for coastal risk management and mangrove conservation policy in Sabah and Sarawak.

## 6. Conclusion

This study provides the first systematic, multi-decadal quantification of the relationship between mangrove loss and coastal flood exposure for the coastlines of Sabah and Sarawak, East Malaysia, covering 1996 to 2020 and projecting forward to 2050 under a structured scenario matrix. Drawing on five publicly available global datasets and a reproducible Python-based analytical workflow, it addresses three research questions.

With respect to the spatial and temporal patterns of mangrove loss, a net decline of 46.34 km² (-1.14%) was recorded within the 10 km coastal buffer over the study period. Whilst this rate is modest relative to regional Southeast Asian averages, gross loss of 114.06 km² indicates that the landscape-level disturbance is substantially greater than the net figure suggests. Loss was concentrated in four principal hotspot regions: Hotspot A (Rajang Delta) and Hotspot B (SW Sarawak coast) in central and southwestern Sarawak, and Hotspot C (Menumbok Forest Reserve) and Hotspot D (Kinabatangan coast) in southwestern and northeastern Sabah respectively, all of which are subject to ongoing oil palm expansion and aquaculture development. A distinct acceleration phase between 2010 and 2016 accounts for the majority of the observed net decline, followed by a partial recovery before the extent reached its lowest recorded value of 4,003.01 km² in 2020.

In terms of the change in flood exposure attributable to mangrove loss, the overlay of hydrologically-connected inundation zones with mangrove loss polygons reveals that 43.79 to 52.14 km² of coastal land, depending on SLR threshold, now lies within the modelled inundation zone having lost its mangrove cover since 1996. This formerly protected area is estimated to shelter approximately 10,200 to 12,730 people who are now exposed to coastal inundation risk without natural buffering. A further 72.16 to 101.88 km² of the inundation zone retains active mangrove cover as of 2020, continuing to provide biophysical protection to an estimated 32,600 to 51,400 coastal residents. The quantified loss-to-exposure ratio of 0.42 km² of flood exposure per km² of mangrove loss provides an empirical basis for translating future mangrove loss projections into flood exposure estimates.

With respect to forward-looking projections to 2050, the scenario matrix reveals that the trajectory of mangrove loss is a more consequential determinant of 2050 coastal flood exposure than the choice of emissions scenario over the same horizon. Under the IPCC AR6 regional median projections for SSP2-4.5 and SSP5-8.5, the difference in projected flood exposure attributable to SLR scenario choice alone is approximately 1.2 km² and approximately 500 people. By contrast, the difference between the low and high mangrove loss trajectories within either SLR scenario is approximately 29 km² and 12,400 people. This result reflects the convergence of the two SLR projections at the 2050 horizon (0.20 m vs 0.23 m regionally) and the continuous compounding of mangrove loss from the present day. In the worst case scenario (SSP5-8.5, high mangrove loss), approximately 570.4 km² of coastal land and 238,200 people are projected to lie within the flood exposure zone by 2050.

Taken together, these findings carry a clear implication for coastal management in East Malaysia. Within the near-term planning horizon to 2050, conservation and restoration of the existing mangrove belt represents the most immediately actionable lever available for reducing coastal flood exposure. The residual mangrove stock currently protecting over 72 km² of inundation-susceptible coastline and tens of thousands of coastal residents should be regarded as functioning natural infrastructure, the loss of which would translate directly and quantifiably into increased flood exposure. Targeted protection of all four identified hotspots — the Rajang Delta, SW Sarawak coast, Menumbok Forest Reserve and Kinabatangan coast — where gross loss has been most severe and where inundation-susceptible lowlands are most extensive, warrants priority attention from both state forestry authorities and coastal risk management agencies.

Future work should address several limitations identified in this study. Substitution of the Copernicus GLO-30 digital surface model with a bare-earth terrain model such as CoastalDEM would reduce elevation uncertainty in vegetated coastal areas. Integration of physics-based hydrodynamic modelling would replace the static bathtub approach with a more physically realistic representation of flood dynamics. Incorporation of projected population growth would improve the robustness of future population exposure estimates. Finally, plot-level

land-use change data linked to the mangrove loss hotspots would enable more rigorous causal attribution of observed loss patterns to specific drivers.

The analytical framework and open-source codebase developed in this study are directly transferable to other mangrove-holding coastlines across the Indo-Pacific where similar data constraints apply. In a region where coastal populations are growing, sea levels are rising, and mangrove loss continues despite improved monitoring, the capacity to quantify the flood exposure consequences of ecosystem change using freely available data represents a meaningful contribution to evidence-based coastal adaptation planning.

## Acknowledgements

The author gratefully acknowledges the providers of the freely available datasets used in this study: the Global Mangrove Watch dataset (GMW v3.0) made available through JAXA and the Global Mangrove Alliance; the Copernicus DEM GLO-30 provided by the European Space Agency and Airbus; the WorldPop Global High Resolution Population dataset provided by the University of Southampton; and the IPCC AR6 Sea Level Projection Tool maintained by NASA Jet Propulsion Laboratory. The analysis was conducted independently, and the findings, interpretations, and conclusions expressed in this paper are those of the author alone.

## Data availability

All derived geospatial datasets, tabular outputs, and analysis code supporting this study are openly available on Zenodo at https://doi.org/10.5281/zenodo.20620479 under a Creative Commons Attribution 4.0 International licence. Raw input datasets are publicly available from their respective providers: GMW v3.0 (https://www.globalmangrovewatch.org/), Copernicus DEM GLO-30 (https://doi.org/10.5270/ESA-c5d3d65), WorldPop (https://www.worldpop.org/), and GADM v4.1 (https://gadm.org/).

## Declaration of Competing Interest

The author declares that there are no conflicts of interest with respect to the research, authorship, or publication of this article. No financial or personal relationships with any organisation or individual have influenced the work reported herein. This research received no external funding.

## Ethics Statement

This research did not involve human participants, animal subjects or any form of clinical intervention. All datasets used are publicly available. Ethical approval was not required and is not applicable for this study.

## References

[1] Reimann L, Vafeidis AT, Honsel LE. Population development as a driver of coastal risk: Current trends and future pathways. *Cambridge Prisms: Coastal Futures*. 2023;1:e14. doi:10.1017/cft.2023.3

[2] Menéndez, P., Losada, I.J., Torres-Ortega, S., Narayan, S., and Beck, M.W. (2020). The global flood protection benefits of mangroves. *Scientific Reports*, 10, 4404. https://doi.org/10.1038/s41598-020-61136-6

[3] Temmerman, S., Horstman, E.M., Krauss, K.W., Mullarney, J.C., Pelckmans, I., and Schoutens, K. (2023). Marshes and mangroves as nature-based coastal storm buffers. *Annual Review of Marine Science*, 15, 95–118. https://doi.org/10.1146/annurev-marine-040422-092951

[4] Malaysia Biodiversity Information System (MyBIS) (2015). Marine and coastal biodiversity. Available at: https://www.mybis.gov.my/art/6 [Accessed: 15 May 2026]

[5] Worthington, T.A., Andradi-Brown, D.A., Bhargava, R., Buelow, C., Bunting, P., Duncan, C., Fatoyinbo, L., Friess, D.A., Goldberg, L., Hilarides, L., Lagomasino, D., Landis, E., Lyons, M.B., Murdiyarso, D., Phinn, S., Rebelo, L.M., Rosenqvist, A., Spalding, M., and Thomas, N. (2020). Harnessing big data to support the conservation and rehabilitation of mangrove forests globally. *One Earth*, 2(5), 429–443. https://doi.org/10.1016/j.oneear.2020.04.018

[6] Kulp, S.A. and Strauss, B.H. (2019). New elevation data triple estimates of global vulnerability to sea-level rise and coastal flooding. *Nature Communications*, 10, 4844. https://doi.org/10.1038/s41467-019-12808-z

[7] Knapp, K.R., Kruk, M.C., Levinson, D.H., Diamond, H.J., and Neumann, C.J. (2010). The International Best Track Archive for Climate Stewardship (IBTrACS): Unifying tropical cyclone data. *Bulletin of the American Meteorological Society*, 91(3), 363–376.

[8] University of California Davis (2023). *Global Administrative Areas (GADM), Version 4.1*. Available at: https://gadm.org [Accessed: 28 February 2026]

[9] Copernicus DEM (2021). *Copernicus Digital Elevation Model (COP-DEM) GLO-30, Product Handbook*. European Space Agency / Airbus DS. Available at: https://registry.opendata.aws/copernicus-dem/ [Accessed: 2 March 2026]

[10] WorldPop (2020). *Global High Resolution Population Denominators Project — Funded by The Bill and Melinda Gates Foundation (OPP1134076)*. University of Southampton. https://doi.org/10.5258/SOTON/WP00675

[11] Fox-Kemper, B., Hewitt, H.T., Xiao, C., Aðalgeirsdóttir, G., Drijfhout, S.S., Edwards, T.L., Golledge, N.R., Hemer, M., Kopp, R.E., Krinner, G., Mix, A., Notz, D., Nowicki, S., Nurhati, I.S., Ruiz, L., Sallée, J.B., Slangen, A.B.A., and Yu, Y. (2021). Ocean, cryosphere and sea level change. In: Masson-Delmotte, V., et al. (eds.), *Climate Change 2021: The Physical Science Basis. Contribution of Working Group I to the Sixth Assessment Report of the Intergovernmental Panel on Climate Change*, Chapter 9. Cambridge University Press. https://doi.org/10.1017/9781009157896.011

[12] Bunting, P., Rosenqvist, A., Hilarides, L., Lucas, R.M., Thomas, N., Tadono, T., Worthington, T.A., Spalding, M., Murray, N.J., and Rebelo, L.M. (2022). Global mangrove extent change 1996–2020: Global Mangrove Watch version 3.0. *Remote Sensing*, 14(15), 3657. https://doi.org/10.3390/rs14153657

[13] NASA Sea Level Change Team (2022). *NASA Team's Sea Level Change Tool — IPCC AR6 Sea Level Projection Tool*. Jet Propulsion Laboratory, California Institute of Technology. Available at: https://sealevel.nasa.gov/ipcc-ar6-sea-level-projection-tool [Accessed: 7 March 2026]

[14] Friess, D.A., Rogers, K., Lovelock, C.E., Krauss, K.W., Hamilton, S.E., Lee, S.Y., Lucas, R., Primavera, J., Rajkaran, A., and Shi, S. (2019). The state of the world's mangrove forests: Past, present, and future. *Annual Review of Environment and Resources*, 44, 89–115. https://doi.org/10.1146/annurev-environ-101718-033302

[15] Spalding, M., Ruffo, S., Lacambra, C., Meliane, I., Hale, L.Z., Shepard, C.C., and Beck, M.W. (2014). The role of ecosystems in coastal protection: Adapting to climate change and coastal hazards. *Ocean and Coastal Management*, 90, 50–57. https://doi.org/10.1016/j.ocecoaman.2013.09.007

[16] Goldberg, L., Lagomasino, D., Thomas, N., and Fatoyinbo, T. (2020). Global declines in human‐driven mangrove loss. *Global Change Biology*, 26(10), 5844–5855. https://doi.org/10.1111/gcb.15275

[17] Lovelock, C.E., Cahoon, D.R., Friess, D.A., Guntenspergen, G.R., Krauss, K.W., Reef, R., Rogers, K., Saunders, M.L., Sidik, F., Swales, A., Saintilan, N., Thuyen, L.X., and Triet, T. (2015). The vulnerability of Indo-Pacific mangrove forests to sea-level rise. *Nature*, 526(7574), 559–563. https://doi.org/10.1038/nature15538

[18] Richards, D.R. and Friess, D.A. (2016). Rates and drivers of mangrove deforestation in Southeast Asia, 2000–2012. *Proceedings of the National Academy of Sciences of the United States of America*, 113(2), 344–349. https://doi.org/10.1073/pnas.1510272113

[19] Van Wesenbeeck, B.K., van Zelst, V.T.M., Antolinez, J.A.A., and de Boer, W.P. (2025). Quantifying uncertainty in wave attenuation by mangroves to inform coastal green belt policies. *Communications Earth and Environment*. https://doi.org/10.1038/s43247-025-02178-4

[20] Sanders, B.F., et al. (2024). Flooding is not like filling a bath. *Earth's Future*, 12. https://doi.org/10.1029/2024EF005164